Strain rate concentration and dynamic stress concentration for double-edge-notched specimens subjected to high-speed tensile loads

N.-A. NODA, H. OHTSUKA, H. ZHENG, Y. SANO, M. ANDO, T. SHINOZAKI and W. GUAN

Department of Mechanical Engineering, Kyushu Institute of Technology, 1-1, Sensui-cho, Tobata, Kitakyushu 804-8550, Japan

ABSTRACT   Engineering plastics provide superior performance to ordinary plastics for wide range of the use. For polymer materials, dynamic stress and strain rate may be major factors to be considered when the strength is evaluated. Recently, high-speed tensile test is being recognized as a standard testing method to confirm the strength under dynamic loads. In this study, therefore, high-speed tensile test is analysed by the finite element method; then, the maximum dynamic stress and strain rate are discussed with varying the tensile speed and maximum forced displacement. The maximum strain rate increases with increasing the tensile speed u/t, but the strain rate concentration factor $K_{t\dot{\varepsilon}}(t) = \dot{\varepsilon}_{yA}(t)/\dot{\varepsilon}_{ynom}(t)$ is found to be constant independent of tensile speed, which is defined as the maximum strain rate $\dot{\varepsilon}_{yA,\,\mathrm{max}}$ appearing at the notch root over the average nominal strain rate at the minimum section $\dot{\varepsilon}_{ynom}(t)$. It is found that the strain rate at the notch root depends on the dynamic stress rate at the notch root and independent of the notch root radius ρ. It is found that the difference between the static and dynamic maximum stress concentration $(\sigma_{yA,\mathrm{max}} - \sigma_{yA,st})$ at the notch root is proportional to the tensile speed when $u/t = 5000\,\mathrm{mm/s}$. Strain rate concentration factors are also discussed with varying the notch depth and specimen length. Based on the elastic strain rate concentration factor, the master curve is obtained useful for understanding the impact fracture of polycarbonate for the wide range of temperature and impact speed.

Keywords   dynamic stress; finite element method; notch; strain rate; stress concentration; Polycarbonate; Time-Temperature Superposition Principle.

NOMENCLATURE		
d	=	width of minimum section in Fig. 1
D	=	width of the specimen in Fig. 1
K_{t0}	=	stress concentration for the semi-infinite plate
$K_{td}(t)$	=	dynamic stress concentration factor defined as $\sigma_{yA}(t)/\sigma_{ynom}(t)$
$K_{t\dot{\varepsilon}}(t)$	=	dynamic strain rate concentration factor defined as $\dot{\varepsilon}_{yA}(t)/\dot{\varepsilon}_{ynom}(t)$
$K_{t\dot{\varepsilon}0}$	=	strain rate concentration for the limiting values $2t/D \rightarrow 0$
L	=	specimen length
t	=	notch depth in Fig. 1
$u(t)$	=	displacement at the time in the y-direction at the fixed end
u_{max}	=	maximum displacement at the fixed end
$\dot{\varepsilon}_{const}^{smooth} = \dfrac{u/t}{L}$	=	converged strain rate of smooth specimen in Fig. 18
$\dot{\varepsilon}_{yA}(t)$	=	strain rate at the notch root A at the time t
$\dot{\varepsilon}_{yA,const}$	=	converged strain rate at the notch root A in Figs 8 and 9
$\dot{\varepsilon}_{yA,\,\mathrm{max}}$	=	maximum strain rate at the notch root A in Figs 8 and 9
$\dot{\varepsilon}_{ynom}(t)$	=	average strain rate at the minimum section
$\dot{\varepsilon}_{ynom,const}$	=	converged average strain rate at minimum section in Fig. 17
ρ	=	notch root radius in Fig. 1
$\sigma_{yA}(t)$	=	dynamic stress at the notch root A at the time t
$\sigma_{yA,st}$	=	static stress at the notch root A
$\sigma_{yA,\mathrm{max}}$	=	maximum dynamic stress at the notch root A in Figs 5 and 6
$\dot{\sigma}_{yA,\,\mathrm{max}}$	=	maximum dynamic stress rate at the notch root A in Fig. 11
$\sigma_{ynom}(t)$	=	average dynamic stress at the minimum section

Correspondence: N.-A. Noda. E-mail: noda@mech.kyutech.ac.jp

INTRODUCTION

Engineering plastics are widely used in everyday products. Typically, an engineering plastic is chosen for its range of enhanced physical properties. For example, polycarbonate has superior impact resistance compared with other polymers or indeed compared with some structural metals.[1] Most thermoplastics far blow their glass transition give a brittle fracture when deformed in uniaxial tension. Polycarbonate is an exception and deforms in a ductile manner. However, Izod impact studies for notched specimens show that the mode of failure changes from ductile to a brittle fracture on annealing samples below T_g. Because the brittle–ductile transition is affected by temperature and loading speed,[2,3] a high-speed tensile test is recently being recognized as a standard testing method. Bluntly notched specimens failed in a fully ductile manner, and sharply notched specimens failed in brittle manner depending on the strain rate at the notch root.

It should be noted that Izod and Charpy impact tests are not suitable for evaluating the impact strength of real products because the impact speeds do not correspond to the real failure. In the high-speed tensile test, it is necessary to obtain the strain rate correctly to understand the impact strength of the polymer specimen. For smooth specimens, the strain rate can be determined as $\dot{\varepsilon}_{const}^{smooth} = u/tL$ from the specimen length L and the tensile speed u/t (Figs 1 & 4). On the other hand, for notched specimens, it is necessary to measure the strain at the notch root by strain gauge measurement, for example. However, because only the average value of the strain concerning the gauge width can be measured, it is not possible to measure the strain at the notch root accurately.

In the previous impact studies, circular holes[4] and elliptical holes[5] were investigated under step load[6,7] and pulse load.[7,8] In addition, review papers are also available for impact problems.[9–11] However, there are few studies on the strain rate concentration for notched specimens under various tensile speed. Therefore, in this paper, the finite element method is applied to analyse the notched specimens under various tensile speed. Then, the dynamic stress concentration factor and the strain rate factor will be discussed with varying tensile speed and maximum values of forced displacement. In this study, to clarify the dynamic stress and strain rate behaviour, the finite element elastic analysis is performed by using the software, FEM code MSC. Marc/Mentat 2011. In order to express dynamic stress oscillation, stiffness matrix multiplier coefficients are obtained by Fourier modal analysis and used in the elastic analysis.[12]
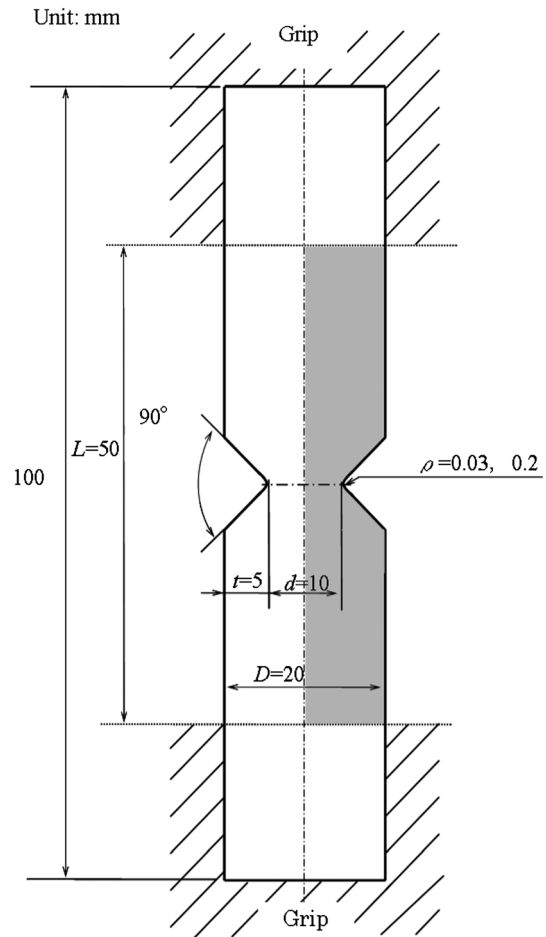

Fig. 1 Geometry of specimen.

STATIC STRESS CONCENTRATION FOR DOUBLE-EDGE-NOTCHED SPECIMENS USED IN HIGH TENSILE LOAD

In this study, the material analysed is assumed as polycarbonate, which has especially high impact strength among the polymeric materials. Young's modulus is assumed as $E = 2.3$ GPa with Poisson's ratio $v = 0.37$. Figure 1 shows the geometry of the double-edge-notched specimen, with dimensions of notch root radius $\rho = 0.03$ and 0.2 mm, notch depth $t = 5$ mm and opening angle 90°. The notch root radius $\rho = 0.03$ mm corresponds to the radius of fillet appearing at polymer products generally. The notch root radius $\rho = 0.2$ mm corresponds to the radius of the notched specimens used in the Izod and Charpy test. When the high-speed tensile test is performed, both ends of the specimen are gripped by rigid chuck; then, forced displacement is applied to the end under constant speed. Figure 2 shows FEM models for analysis. Here, model 1 has the notch radius $\rho = 0.03$ mm, and model 2 has
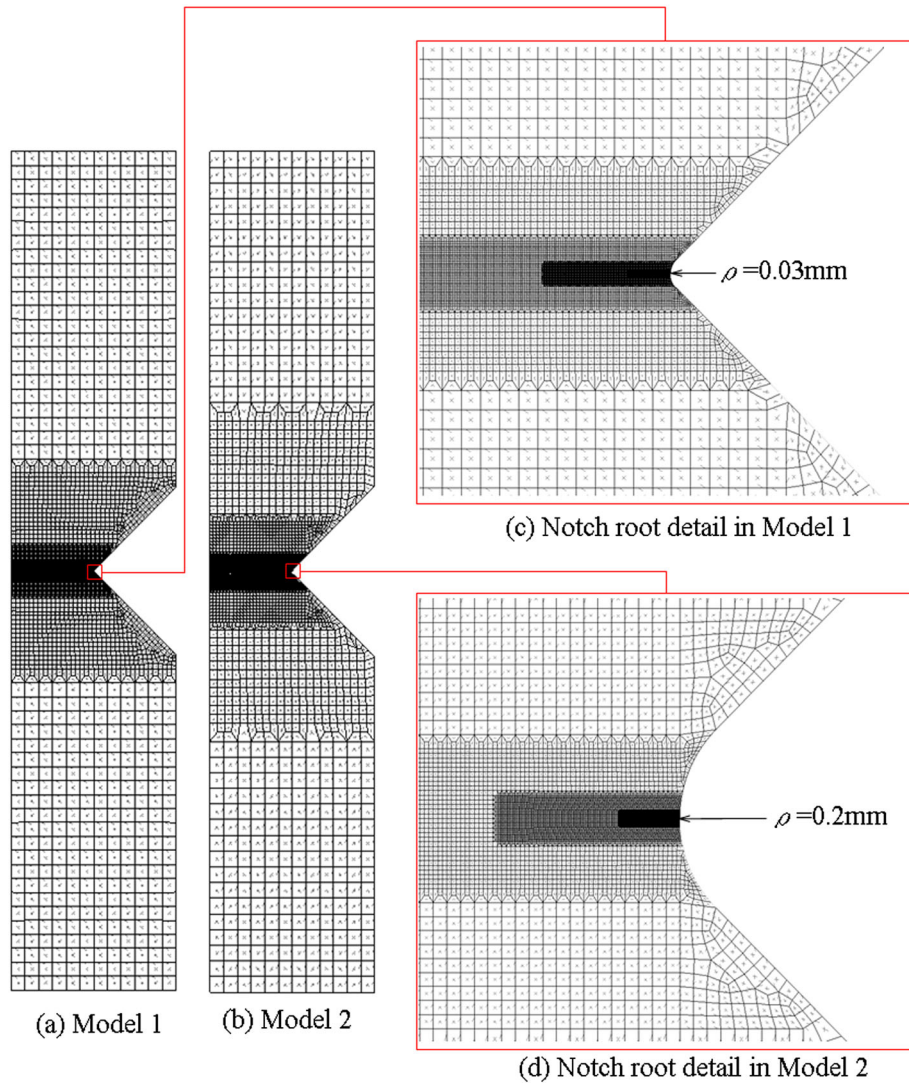
Fig. 2 FEM models. (a) Model 1, (b) Model 2, (c) notch root detail in Model 1 and (d) notch root detail in Model 2.

$\rho = 0.2$ mm. Figure 2c shows the notch root detail in model 1, and Fig. 2d shows the notch root detail in model 2. Minimum mesh size of the notch root is $e = \rho/243$ each model. Figure 3 shows the boundary conditions given to the end portion of the analysis models. Figure 3a shows boundary conditions in the rigid chucks, and Fig. 3b shows a tensile stress boundary conditions generally used. Table 1 shows the effect of the difference in the boundary conditions on the static stress concentration factor. From Table 1, the stress concentration factor is almost the same in the tension by rigid chucks and the uniform tensile stress for the span length as shown in Fig. 1. Also, Table 1, results using the model of Fig. 2, shows less than 1% error with respect to the exact stress concentration factor calculated by the approximate

expression.[13–17] Thus, models 1 and 2 are found to provide high accuracy. In the dynamic analysis, time step interval also affects the accuracy of the results. In this analysis, the time step 1×10^6 is found to be enough to obtain 3-digit-accuracy.[18] In a transient dynamic analysis, damping represents the dissipation of energy in the structural system. In FEM code MSC. Marc/Mentat 2011, the programme bases integration on the usual assumption that the damping matrix of the system is a linear combination of the mass and stiffness matrices. Element damping uses coefficients on the element matrices and is represented by the equation
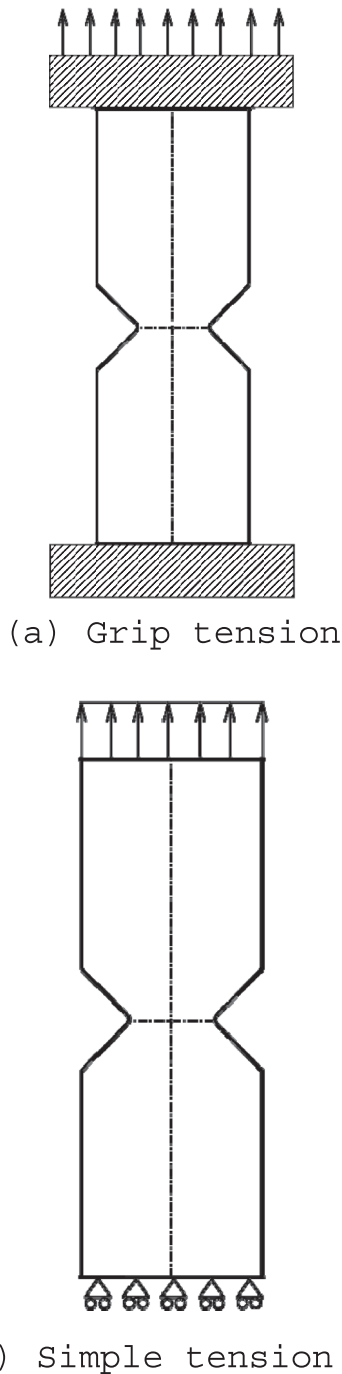
$$[C] = \alpha[M] + \beta[K] \tag{1}$$

(a) Grip tension

(b) Simple tension

Fig. 3 Boundary conditions. (a) Grip tension and (b) Simple tension.

Table 1 Static stress concentration factor by FEM

Notch (mm)	K_{ts} in Fig. 3a	K_{ts} in Fig. 3b	References [13–17] in Fig. 3b
$\rho = 0.03$, $t = 5$	14.46	14.48	14.49
$\rho = 0.2$, $t = 5$	6.14	6.15	6.12

Here, $[C]$ is the global damping matrix, $[M]$ is the mass matrix and $[K]$ is the stiffness matrix. Because of the same damping coefficients are used throughout the structure, the following equation can be used to obtain the mass damping coefficient α and the usual stiffness damping coefficient β. The mass damping coefficient and the usual stiffness damping coefficient will be used for the dynamic analysis.

$$\zeta = \frac{1}{2}\left(\frac{\alpha}{\omega} + \beta\omega\right) \tag{2}$$

Here, ζ is the damping ratio, and ω is the frequency which can be calculated by FEM.

DYNAMIC STRESS CONCENTRATION FOR HIGH-SPEED TENSILE TEST SPECIMENS

Figure 4 shows the forced displacement u given at the end of the specimen. The average stress σ_{gross} is also indicated, which is expressed as $\sigma_{gross}(t) = 0.867\mathrm{E} \cdot u(t)/L$ from FEM analysis. The nominal stress at the minimum

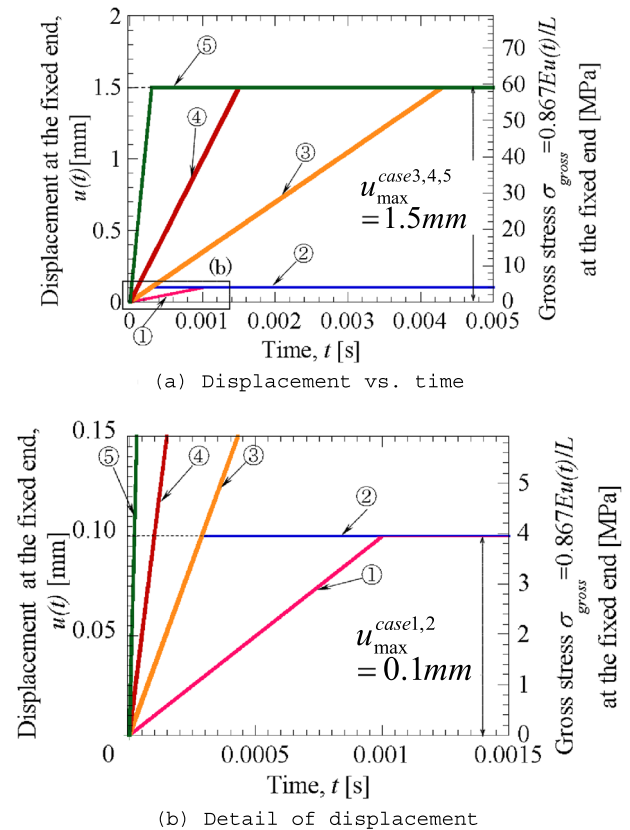(a) Displacement vs. time

(b) Detail of displacement

Fig. 4 Loading conditions defined as Case 1 to Case 5 shown as ①-⑤. (a) Displacement versus time and (b) detail of displacement.

Table 2 Displacement u at the grip end

Case in Fig 4			1	2	3	4	5
Condition	Maximum displacement	u_{max}	0.1 mm $t = 0.00100$ s	0.1 mm $t = 0.00029$ s	1.5 mm $t = 0.00429$ s	1.5 mm $t = 0.00150$ s	1.5 mm $t = 0.00030$s
	Tensile speed	u/t	100 mm/s $t < 0.00100$ s	350 mm/s $t < 0.00029$ s	350 mm/s $t < 0.00429$ s	1000 mm/s $t < 0.00150$ s	5000 mm/s $t < 0.00030$ s

section is expressed as $\sigma_{rest} = (D/d)\sigma_{gross}$. Here, we mainly consider 5 cases, as shown in Table 2. Table 2 shows the tensile speed, the maximum forced displacement of the fixed end and the time of that appear. In case 5, the tensile speed $u/t = 5000$ mm/s corresponds to the impact speed when someone dropped a cell phone to the ground. The maximum displacement 1.5 mm correspond to the brittle fracture appearing at high-speed tensile test. The maximum displacement 0.1 mm corresponds to the case of nondestructive for high-speed tensile test.

Figures 5 and 6 show the dynamic stress at the notch root A for cases 1–5. Also, Figs 5 and 6 show the detail of the dynamic stress oscillation with each case. From Figs 4 and 5, it is seen that the maximum dynamic stress $\sigma_{yA,max}$ appears at almost the same time of the maximum forced displacement, defined as the maximum value of dynamic stress $\sigma_{yA,max}$ in each case. After several oscillations due to the stress wave, dynamic stress

approaches static stress $\sigma_{yA,st}$. From the comparison between case 1 and case 2, it is shown that the maximum dynamic stress oscillation ($\sigma_{yA,max} - \sigma_{yA,st}$) at the notch root point A in case is larger than that in case 1. From the comparison between case 2 and case 3, it is seen that of the same maximum dynamic stress oscillation ($\sigma_{yA,max} - \sigma_{yA,st}$) at the notch root point A is observed although the final displacement of case 3 is 15 times larger than that in case 2. It is may be concluded that the maximum dynamic stress oscillation ($\sigma_{yA,max} - \sigma_{yA,st}$) is controlled by the tensile speed.

Figure 7 shows the relationship between the tensile speed u/t and ($\sigma_{yA,max} - \sigma_{yA,st}$) for $\rho = 0.03$ and 0.2 mm. Here, the results for $u/t = 100\,000$, $1\,000\,000$ mm/s and step load $u/t = \infty$ are also indicated when the maximum displacement is 1.5 mm. It is seen that ($\sigma_{yA,max} - \sigma_{yA,st}$) is proportional to the tensile speed when $u/t \leq 5000$ mm/s. However, ($\sigma_{yA,max} - \sigma_{yA,st}$) becomes constant when $u/t \geq 100\,000$ mm/s. This is
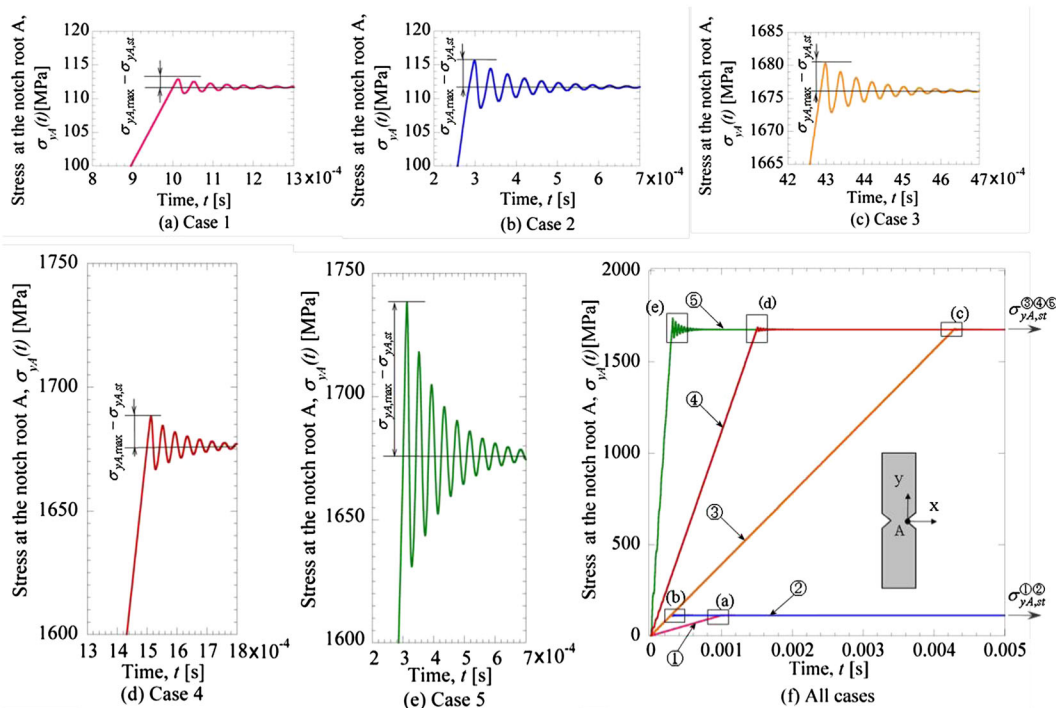

Fig. 5 Dynamic stress at notch root A when $\rho = 0.03$ mm for (a) Case 1, (b) Case 2, (c) Case 3, (d) Case 4, (e) Case 5 and (f) all Cases. Case 1 to Case 5 as shown ①-⑤ in Fig. 4.
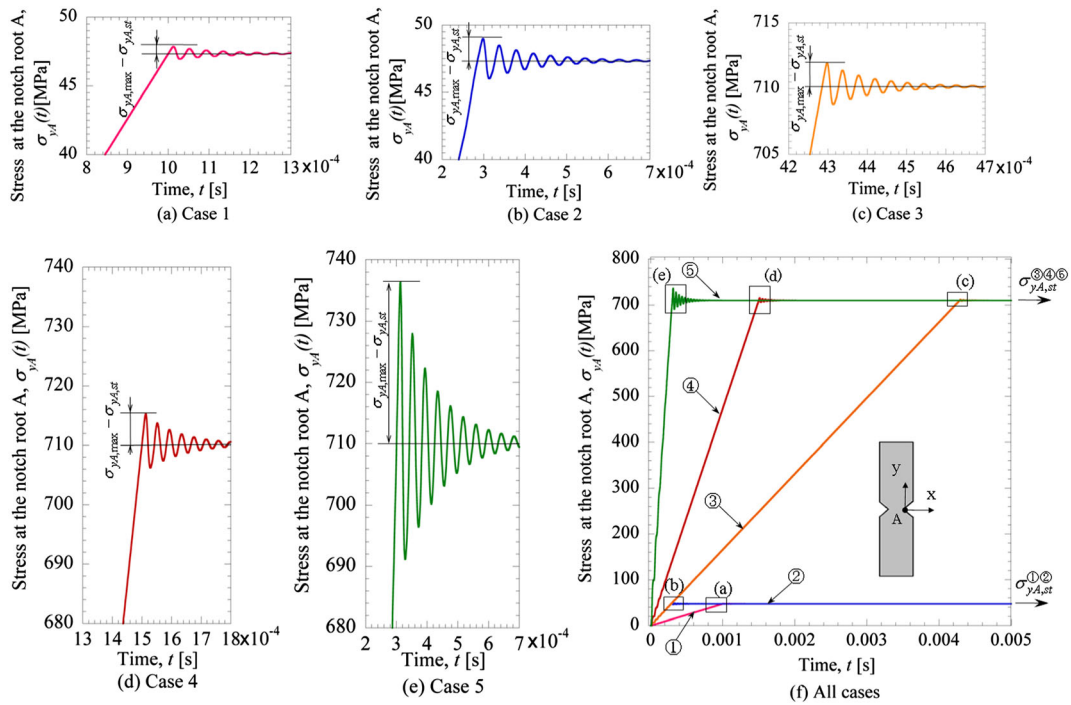
Fig. 6 Dynamic stress at notch root A when $\rho = 0.2$ mm for (a) Case 1, (b) Case 2, (c) Case 3, (d) Case 4, (e) Case 5 and (f) all cases. Case 1 to Case 5 as shown ①-⑤ in Fig. 4.
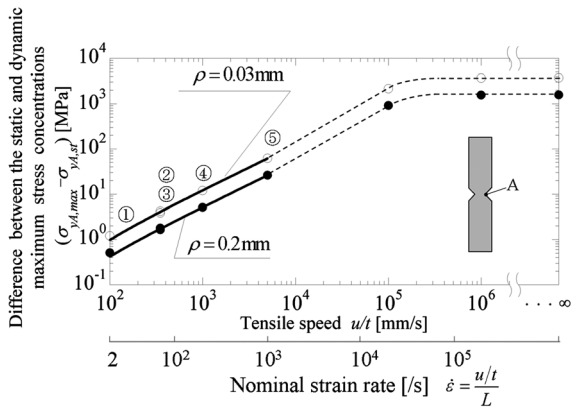

Fig. 7 Difference between the static and dynamic maximum stress concentrations $(\sigma_{yA,\max} - \sigma_{yA,st})$.

related to the fact that stress wave propagation speed is equal to the sonic wave propagation speed. Here, $u/t \geq 100\,000$ mm/s corresponds to the automobile crashing speeds.

STRAIN RATE CONCENTRATION FOR HIGH-SPEED TENSILE TEST SPECIMEN

Figures 8 and 9 show the strain rate at the notch root A for cases 1–5 in Fig. 4. The strain rate increases

dramatically at the start of applying forced displacement. Then, after several oscillations, the strain rate becomes constant. After stopping the forced displacement, several oscillations appear again; then, it eventually converges to zero. From the comparison between case 3 and case 4, it is seen that the same maximum strain rate $\dot{\varepsilon}_{yA,\max}$ and the same converged strain rate $\dot{\varepsilon}_{yA,const}$ are observed although the final displacement $u_{\max}$ of case 3 is 15 times larger than that in case 2. It may be concluded that the strain rate concentration is controlled by the tensile speed.

Figure 10 shows the relationship between the tensile speed u/t and the strain rate for $\rho = 0.03$ and 0.2 mm. Here, the results for $u/t = 100\,000$, $1\,000\,000$ mm/s and step load $u/t = \infty$ are also indicated when the maximum displacement is 1.5 mm. It is seen that the strain rate is proportional to the tensile speed when $u/t \leq 5000$ mm/s. However, the strain rate becomes constant when $u/t \leq 100\,000$ mm/s.

Figure 10 shows that the maximum strain rate $\dot{\varepsilon}_{yA,\max}$ is controlled by the tensile speed that is the nominal strain rate at the fixed end. Next, we focus on the relationship at the notch root A. Figure 11 shows the relationship between the strain rate at the notch root and the dynamic stress rate at the notch root $\dot{\sigma}_{yA,\max}$ when the radius is 0.2 and 0.03 mm. The dynamic stress at the notch root is the value
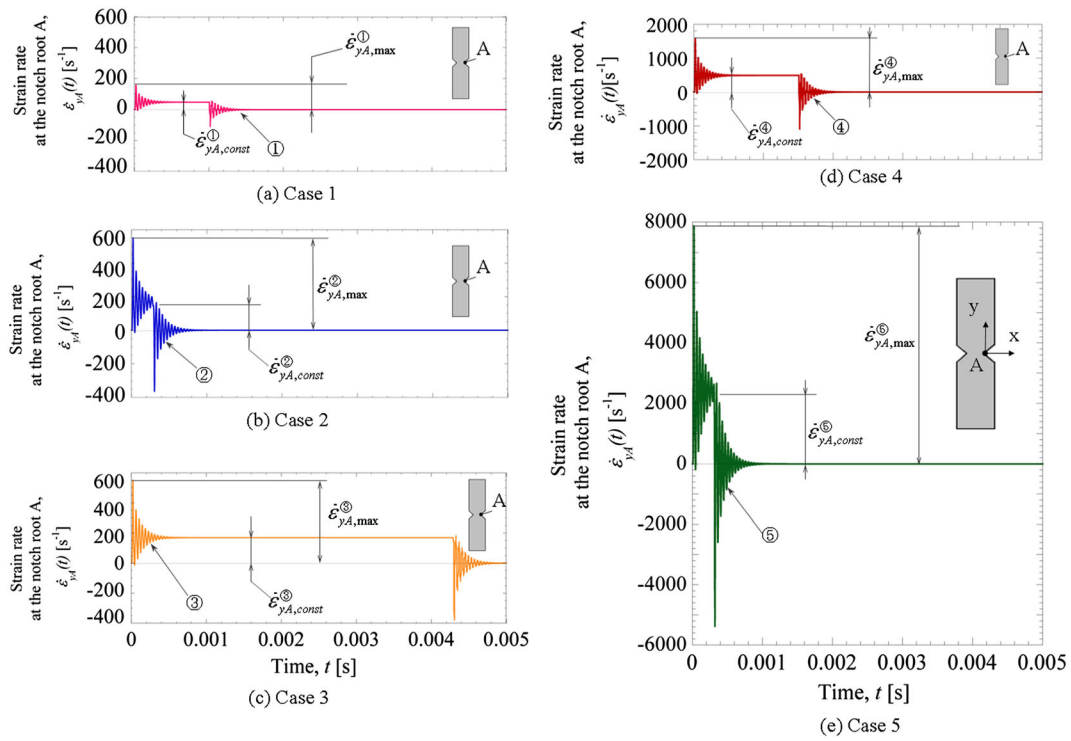
Fig. 8 Strain rate at notch root A when $\rho = 0.03$ mm for (a) Case 1, (b) Case 2, (c) Case 3, (d) Case 4 and (e) Case 5 defined in Fig. 4. Case 1 - Case 5 as shown ① - ⑤ in Fig. 4.
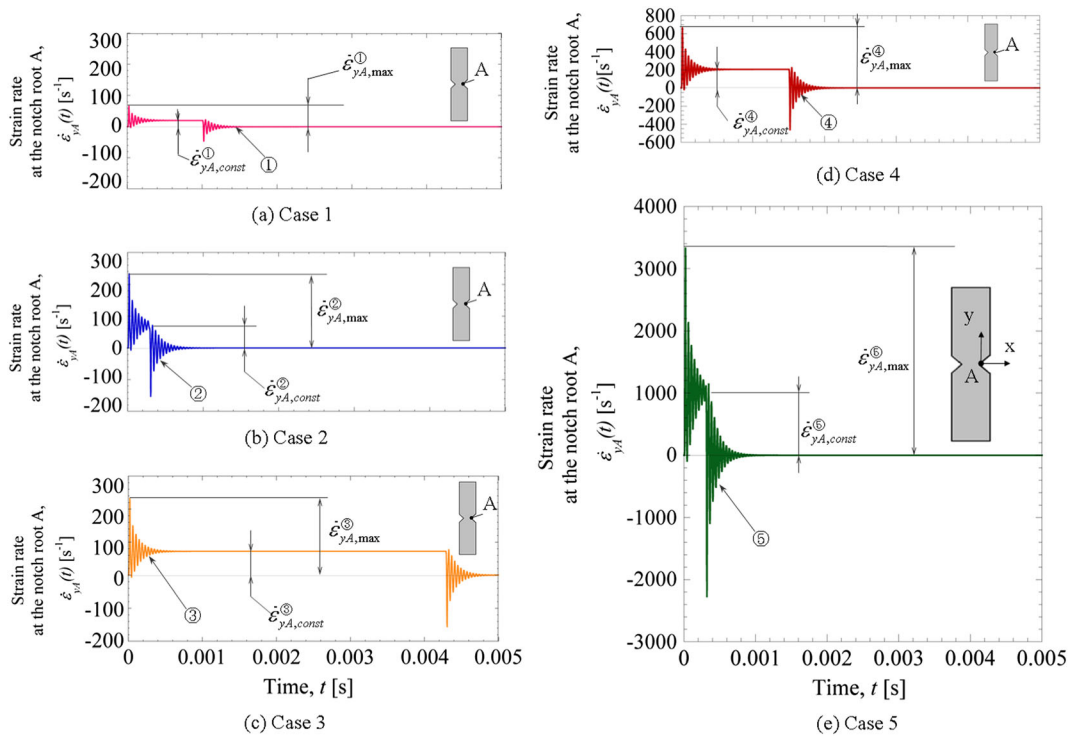

Fig. 9 Strain rate at notch root A when $\rho = 0.2$ mm for (a) Case 1, (b) Case 2, (c) Case 3, (d) Case 4 and (e) Case 5 defined in Fig. 4. Case 1 - Case 5 as shown ① - ⑤ in Fig. 4.
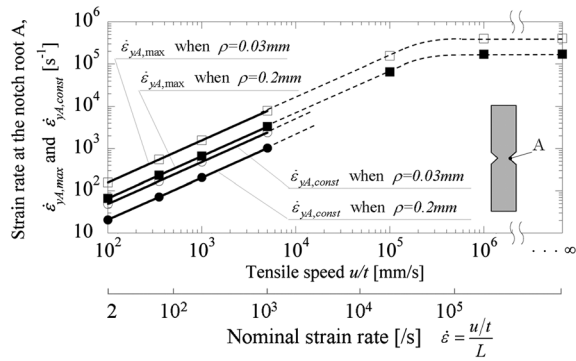
Fig. 10 Maximum strain rate $\dot{\varepsilon}_{yA,\max}$ and converged strain rate $\dot{\varepsilon}_{yA,const}$ versus tensile speed for the notch root radios $\rho = 0.2$ mm and $\rho = 0.3$ mm.
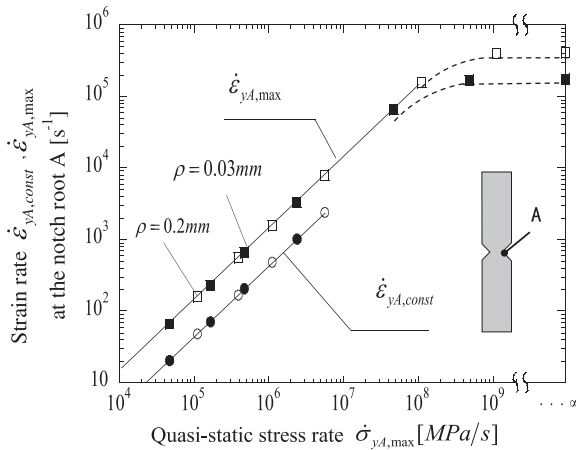

Fig. 11 Maximum strain rate $\dot{\varepsilon}_{yA,\max}$ and converged strain rate $\dot{\varepsilon}_{yA,const}$ versus quasi-static stress rate at the notch root $\dot{\sigma}_{yA,\max}$ useful for all notch radius.

when the strain rate at the notch root becomes to be constant. As shown in Fig. 11, it is found that the strain rate at the notch root is controlled by the dynamic stress rate at the notch root $\dot{\sigma}_{yA,\max}$ and independent of the notch root radius ρ. In this study, $\rho = 0.2$ and $\rho = 0.03$ are considered. However, the results

for any notch root radius ρ can be predicted form Fig. 11 if the dynamic stress rate at the notch root $\dot{\sigma}_{yA,\max}$ can be calculated.

DYNAMIC STRESS DISTRIBUTION AT THE MINIMUM SECTION

Figure 12 shows the dynamic stress distributions at the minimum section when the maximum dynamic stress appears. The dynamic stress concentration factor $K_{td}(t)$ is defined by the maximum dynamic stress $\sigma_{yA,\max}$ at the notch root over the average dynamic stress $\sigma_{y,nom}(t)$ at the minimum section at each time. From Fig. 12, when $\rho = 0.03$ mm, it is seen that the maximum dynamic stress $\sigma_{yA,\max}$ at the notch root is always 14.48 times larger than that of the nominal stress $\sigma_{y,nom}(t)$ at the minimum section at each time for cases 1–5. Similarly, when $\rho = 0.2$ mm, the maximum dynamic stress $\sigma_{yA,\max}$ at the notch root is always 6.43 times larger than that of the nominal stress $\sigma_{y,nom}(t)$ at the minimum section at each time for cases 1–5. The stress concentration factor coincides with the static stress concentration factor obtained by the formula of Murakami and Noda *et al.*[13–17]

Figure 13a shows the maximum dynamic stress $\sigma_{yA,\max}$ at the notch root and nominal dynamic stress $\sigma_{y,nom}(t)$. Figure 13b shows the dynamic stress concentration factor $K_{td}(t)$. It is seen that $K_{td}(t)$ is constant although $\sigma_{yA,\max}$ and $\sigma_{y,nom}(t)$ are changed depending on the time. This is because the maximum dynamic stress at the notch root and the nominal dynamic stress are similarly controlled by the time. It may be concluded that the dynamic stress concentration factor is always constant and controlled by the notch shape alone. Therefore, from the results of the dynamic stress at the minimum section the maximum stress can be determined.

Table 3 and Fig. 14 show the dynamic stress concentration factor with varying $2t/D$. The limiting values for $2t/D \to 0$ correspond to the results for the
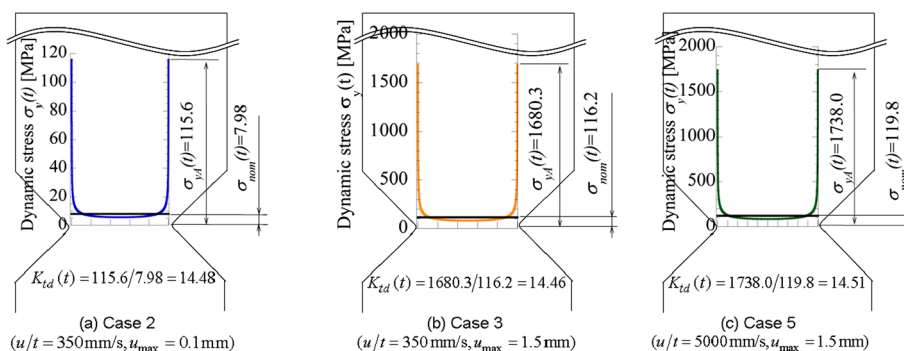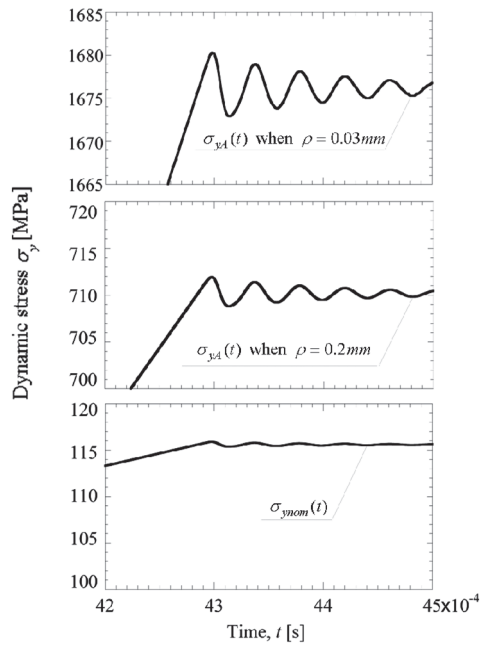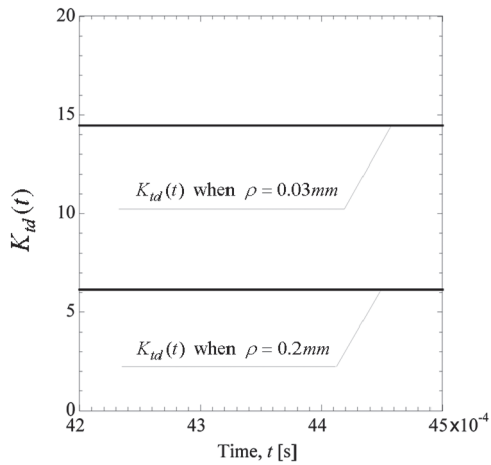

Fig. 12 Dynamic stress distribution along minimum section when the maximum dynamic stress appears for $\rho = 0.02$ mm (a) Case 2 (b) Case 3 (c) Case 5 as defined in Fig. 4.

(a) Dynamic stress at the notch root A
and average dynamic stress
at the minimum section

(b) Strain rate concentration factor

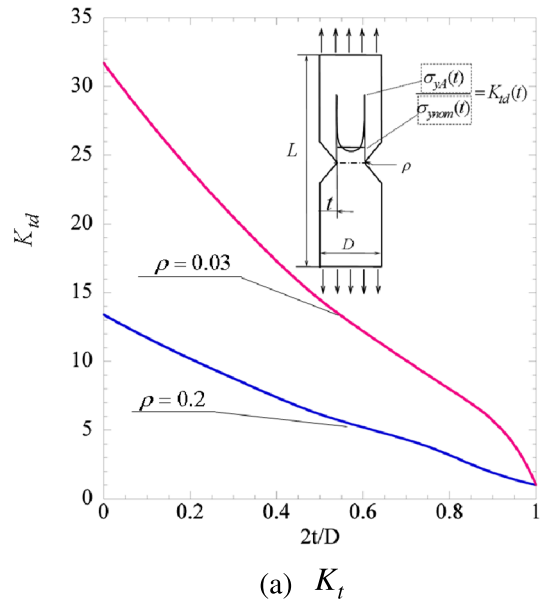**Fig. 13** Constancy of dynamic stress concentration factor.

semi-infinite plate. Figure 14b shows the ratio K_t/K_{t0} where K_{t0} is the results for semi-infinite plate.[13–17] As show in Fig. 14b, the results are independent of the notch root radius.

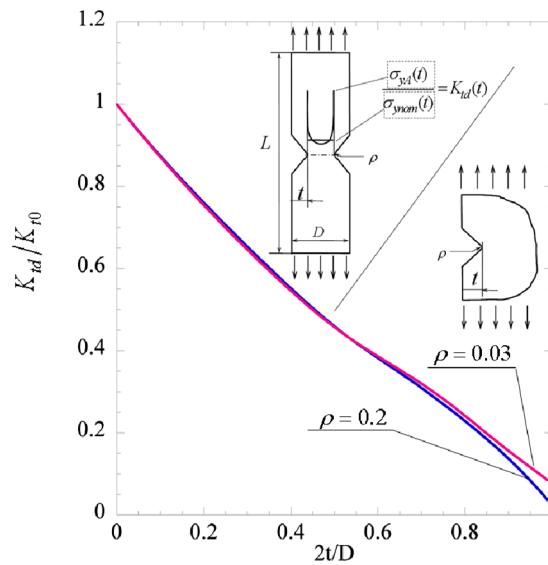## STRAIN RATE DISTRIBUTION AT THE MINIMUM SECTION

Figure 15 shows the strain rate distributions at the minimum section when the maximum strain rate appears.

Table 3 Dynamic stress concentration factor K_{td} and ratio K_{td}/K_{t0} (K_{t0} = the results for semi-infinite plate by Noda et al.[15–17])

		K_t		K_t/K_{t0}	
	ρ (mm)				
t (mm)	$2t/D$	0.2	0.03	0.2	0.03
$\rightarrow 0$	$\rightarrow 0$	13.42	31.71	1	1
1	0.1	11.72	27.62	0.873	0.871
2.5	0.25	9.48	22.16	0.706	0.699
5	0.5	6.14	14.46	0.458	0.456
7.5	0.75	3.84	9.01	0.271	0.284
9	0.9	1.87	5.94	0.139	0.187

(a) K_t

(b) K_t/K_{t0}

Fig. 14 Dynamic stress concentration factor K_{td} (t) versus notch depth $2t/D$ relation.
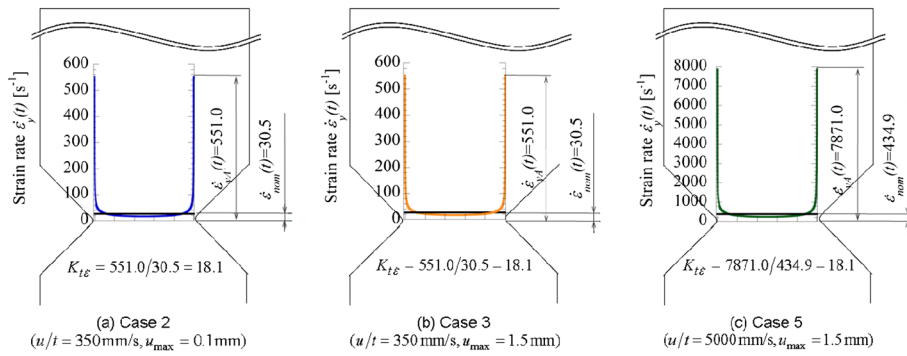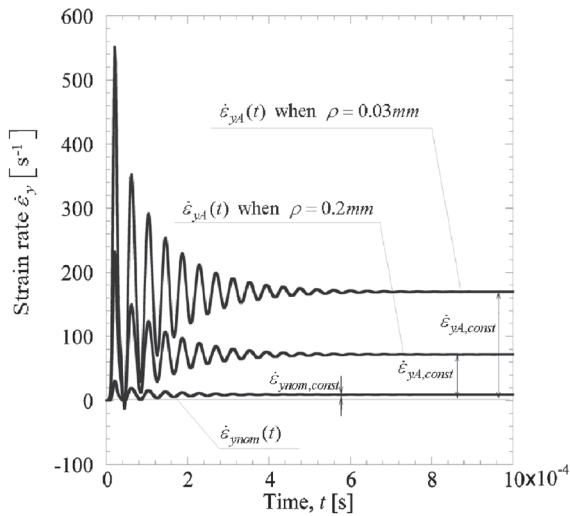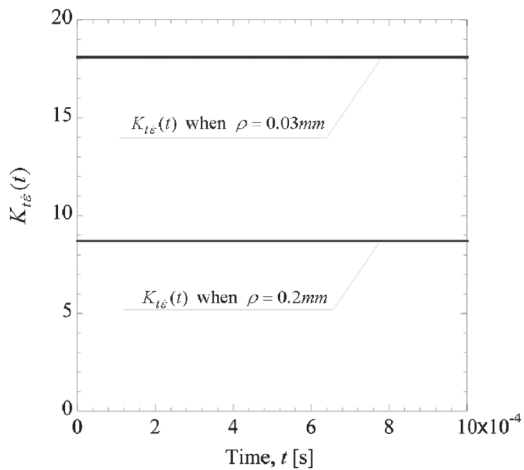
Fig. 15 Strain rate distribution along minimum section when the maximum strain rate appears for $\rho = 0.03$ mm (a) Case 2 (b) Case 3 (c) Case 5.

(a) Dynamic stress at the notch root A and average dynamic stress at the minimum section

(b) Strain rate concentration factor

Fig. 16 Constancy of strain rate concentration factor.

Table 4 Strain rate concentration factor $K_{t\dot{\varepsilon}}$ and ratio $K_{t\dot{\varepsilon}}/K_{t\dot{\varepsilon}0}$ (The limiting values $K_{t\dot{\varepsilon}0}$ for $2t/D \rightarrow 0$ are obtained by the extrapolation from the results for $2t/D = 0.1$ and 0.25.)

| | | $K_{t\dot{\varepsilon}}$ | | $K_{t\dot{\varepsilon}}/K_{t\dot{\varepsilon}0}$ | |
| | ρ (mm) | | | | |
t (mm)	$2t/D$	0.2	0.03	0.2	0.03
$\rightarrow 0$	$\rightarrow 0$	15.55	30.65	1	1
1	0.1	14.05	27.89	0.904	0.910
2.5	0.25	11.82	23.75	0.760	0.755
5	0.5	8.72	18.05	0.561	0.589
7.5	0.75	4.97	11.53	0.320	0.376
9	0.9	3.10	6.88	0.199	0.224

The strain rate concentration factor $K_{t\dot{\varepsilon}}(t)$ is defined by the maximum strain rate $\dot{\varepsilon}_{yA,\max}$ at the notch root over the average strain rate $\dot{\varepsilon}_{y,nom}(t)$ at the minimum section at each time. From Fig. 15, when $\rho = 0.03$ mm, it is seen that the maximum strain rate $\dot{\varepsilon}_{yA,\max}$ at notch root is always 18.1 times larger than that of the nominal strain rate $\dot{\varepsilon}_{y,nom}(t)$ at the minimum section for cases 1–5. Similarly, when $\rho = 0.2$ mm, the maximum strain rate $\dot{\varepsilon}_{yA,\max}$ at the notch root is always 8.72 times larger than that of the nominal strain rate $\dot{\varepsilon}_{y,nom}(t)$ at the minimum section for cases 1–5.

Figure 16a shows the strain rate at the notch root and nominal strain rate. Figure 16b shows the strain rate factor $K_{t\dot{\varepsilon}}(t)$. It is seen that $K_{t\dot{\varepsilon}}(t)$ is constant although $\dot{\varepsilon}_{yA,\max}$ and $\dot{\varepsilon}_{y,nom}(t)$ are changed depending on the time. It may be concluded that the strain rate concentration factor is always constant and controlled by the notch shape alone.

Table 4 and Fig. 17 show the strain rate concentration factor with varying $2t/D$. The limiting values $K_{t\dot{\varepsilon}0}$ for $2t/D \rightarrow 0$ are obtained by the extrapolation from the results for $2t/D = 0.1$, 0.25. As shown in

(a) $K_{t\dot{\varepsilon}}$
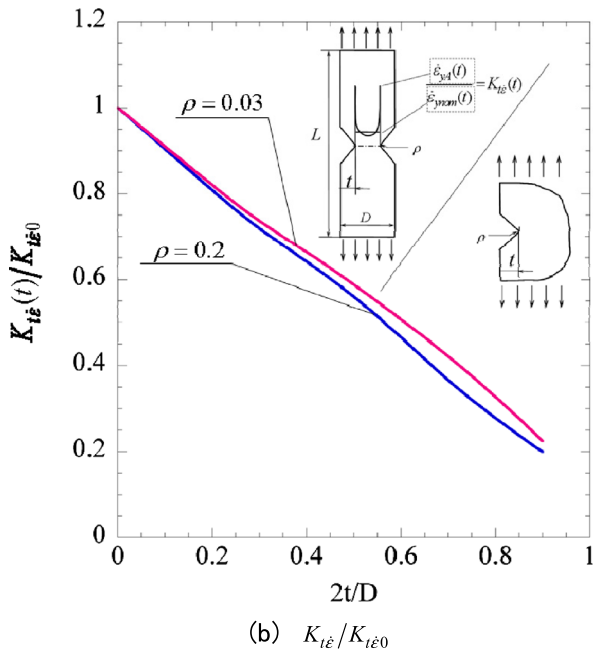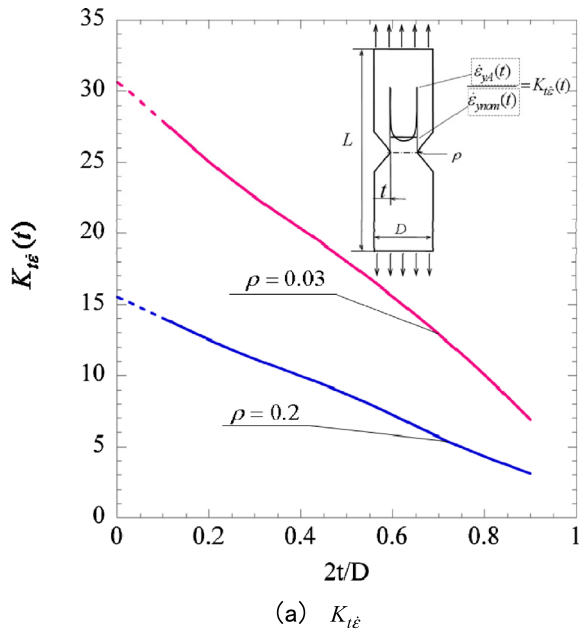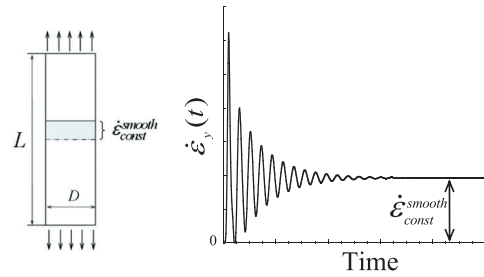

(b) $K_{t\dot{\varepsilon}}/K_{t\dot{\varepsilon}0}$

Fig. 17 Strain rate concentration factor $K_{t\varepsilon}$ versus notch depth $2t/D$ relation.

Fig. 17b, the results are almost independent of the notch root radius.

EFFECT OF SPECIMEN LENGTH UPON THE DYNAMIC STRESS CONCENTRATION AND STRAIN RATE CONCENTRATION

The effect of specimen length on the strain rate $\dot{\varepsilon}_{const,nom}$ is considered. Table 5 shows the results for smooth

Table 5 Converged strain rate $\dot{\varepsilon}_{const}^{smooth}$ for smooth specimen

	$\dot{\varepsilon}_{const}^{smooth}$			
	$L = 25\,mm$	$L = 50\,mm$	$L = 100\,mm$	$L = 200\,mm$
$D = 20\,mm$	14	7	3.5	1.75
$D = 10\,mm$	14	7	3.5	1.75

specimen. It is seen that the strain rate $\dot{\varepsilon}_{const}^{smooth} = \frac{u/t}{L}$ is independent of the width of specimen D. Here, $\dot{\varepsilon}_{const,nom}$ is converged and average strain rate in Fig. 15a. Table 6 and Fig. 18 show the average strain rate $\dot{\varepsilon}_{const,nom}$ with varying $2t/D$ and specimen length L in comparison with the results for plane specimen $\dot{\varepsilon}_{const}^{smooth}$. Figure 18 indicates the ratio $\dot{\varepsilon}_{const,nom}/\dot{\varepsilon}_{const}^{smooth}$. As shown in Fig. 19, with increasing $2t/D$, the ratio $\dot{\varepsilon}_{const,nom}/\dot{\varepsilon}_{const}^{smooth}$ increases. The average strain rate $\dot{\varepsilon}_{const,nom}$ depends on the specimen length as shown in Fig. 19. If the specimen length L is fixed, the average strain rate is independent of the notch root radius ρ as shown in Fig. 15a.

APPLICATION OF THE TIME–TEMPERATURE SUPERPOSITION PRINCIPLE TO POLYCARBONATE

Depending on the test temperature and tensile speed, brittle or ductile fractures are observed for polycarbonate. Figure 20 shows the relationship between the nominal fracture strain and notch root strain rate under various temperatures of polycarbonate, when $\rho = 0.2$mm which is used in Izod and Charpy test. The high strain rate or low temperature causes the brittle fracture. It is known that the time–temperature superposition is frequently applied to determine the temperature dependence of the time or frequency at a given temperature of the polymeric meterial.[19] In this study, the impact properties are considered in terms of the time–temperature superposition principle. Here, the shift factor a_T is obtained at the reference

Table 6 Converged average strain rate $\dot{\varepsilon}_{const,nom}$ for the notched specimen

		$2t/D$	$L = 25$ mm	$L = 50$ mm	$L = 100$ mm	$L = 200$ mm
$\dot{\varepsilon}_{ynom,const}$ $\rho = 0.03$ mm	$\rightarrow 0$	$(\dot{\varepsilon}_{const}^{smooth} =)$	14	7	3.5	1.75
	0.25		14.148	7.375	3.739	1.977
	0.5		15.933	9.294	4.882	2.668
	0.75		25.154	15.938	9.210	4.985
	0.9		50.683	34.813	19.922	12.055
$\dot{\varepsilon}_{ynom,const} / \dot{\varepsilon}_{const}^{smooth}$ $\rho = 0.03$ mm	$\rightarrow 0$	$(\dot{\varepsilon}_{const}^{smooth} =)$	1	1	1	1
	0.25		1.0105	1.1380	1.7967	3.6202
	0.5		1.0535	1.3277	2.2768	4.9732
	0.75		1.0682	1.3948	2.6314	5.6925
	0.9		1.1297	1.5245	2.8485	6.8885

temperature $T_0 = 296$ K and the empirical constants $C_1 = 0.71$, $C_2 = 63.4$.[20]

$$\log a_T = -\frac{C_1(T - T_0)}{C_2 + (T - T_0)} \tag{3}$$

Then, the master curve for the final fracture elongation for polycarbonate is obtained in terms of the strain rate at the notch in conjunction with shift factors. The fracture behaviour can be predicted for the wide range of impact speed under various temperatures from the master curve. Based on the elastic strain rate concentration factor, the master curve is obtained for the wide range as shown in Fig. 21. It is found that the elastic analysis is useful for understanding the impact behaviour of polycarbonate.
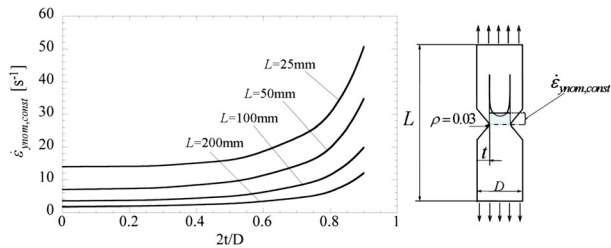

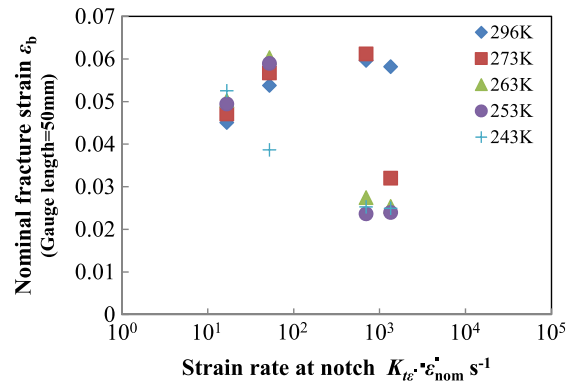**Fig. 18** Converged average strain rate $\dot{\varepsilon}_{const,nom}$ versus notch depth $2t/D$ relation.

Fig. 20 Final fracture strain of polycarbonate obtained under various tensile speed and temperatures when $\rho = 0.2$ mm.
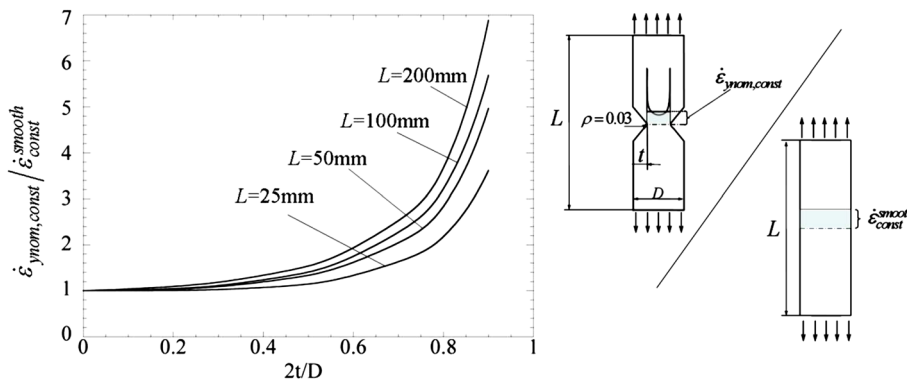

Fig. 19 Ratio $\dot{\varepsilon}_{const,nom} / \dot{\varepsilon}_{const}^{smooth}$ versus notch depth $2t/D$ relation.
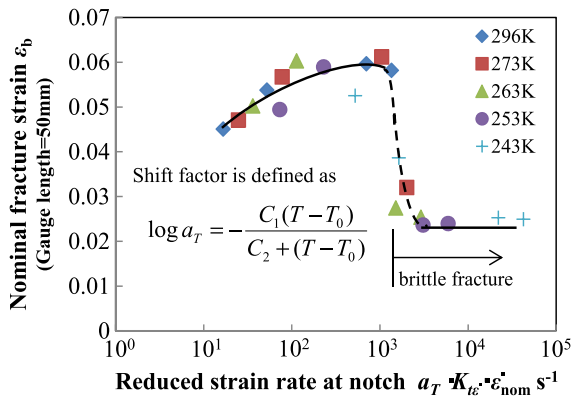
Fig. 21 Master curves for final fracture strain ε_b of polycarbonate expressed in terms of reduced strain rate to predict ductile or brittle fracture for $\rho = 0.2$mm.

CONCLUSIONS

Recently, high-speed tensile test is being used as a standard testing method to evaluate impact strength of the engineering plastics and the other materials. For polymeric material, the strain rate and dynamic stress concentrations are significant factors to be considered in the fracture. However, it is not easy to measure the dynamic stress or strain rate accurately at the notch root by experiment. In this study, therefore, dynamic and elastic FEM is applied to the high-speed tensile test for notched specimens. Then, the dynamic stress and strain rate concentrations have been discussed under various tensile speed. The conclusions can be made the following way.

(1) It may be concluded that the maximum strain rate increases with increasing the tensile speed as shown in Fig. 10. However, the strain rate concentration factor $K_{t\dot{\varepsilon}}(t) = \dot{\varepsilon}_{yA}(t)/\dot{\varepsilon}_{ynom}(t)$ is always constant. Here, the $K_{t\dot{\varepsilon}}$ which is defined by the maximum strain rate $\dot{\varepsilon}_{yA,max}$ at the notch root over the average strain rate $\dot{\varepsilon}_{ynom}(t)$ at the minimum section at each time.

(2) It may be concluded that the dynamic stress concentration factor $K_{td} = \sigma_{yA,max}/\sigma_{y,nom}(t)$ is always constant and controlled by the notch shape alone independent of the tensile speed. The stress concentration factor K_{td} coincides with the static stress concentration factor K_{ts} obtained by the formula in the references.[13–17]

(3) It is found that the difference between the static and dynamic maximum stress concentration $(\sigma_{yA,max} - \sigma_{yA,st})$ at the notch root increases in proportional to the tensile speed when $u/t \le 5000$ mm/s.

(4) It is found that the strain rate at the notch root depends on the quasi-static stress rate at the notch root alone and independent of the notch root radius ρ.

(5) The master curve for the final fracture elongation for polycarbonate can be expressed in terms of the strain rate at the notch in conjunction with shift factors. The fracture behaviour can be predicted for the wide range of impact speed under various temperatures from the master curve.

Acknowledgements

REFERENCES

1 Radin, J., Goldsmith, W. (1988) Normal missile penetration and perforation of layered plates. *Int. J. Impact Eng.*, **7**, 229–259.
2 Aya, T., Nakayama, T. (1995) Influence of strain rate on elastic modulus of polymers. Journal of the Japan Society for Technology of Plasticity. *Sosei-to-Kako*, **36**, 665–670.
3 Honma, S. (2004) Practical strength and durability of plastics (in Japanese). *Plastics*, **55**, 174–182.
4 Chatani, A., Uchiyama, S. (1972) Dynamic stress concentration of notched strips. *Material*, **21**, 636–640.
5 Altenhof, W., Zamani, N., North, W., Arnold, B. (2004) Dynamic stress concentrations for an axially loaded strut at discontinuities due to an elliptical hole or double circular notches. *Int. J. Impact Eng.* **30**, 255–274.
6 Kawata, K., Hashimoto, S. (1972). Dynamic stress concentration for notched elastic bar under dynamic load. *ISAS report University of Tokyo (in Japanese)*, **8**, 377–384.
7 Matsumoto, H., Nakahara, I. (1966) Dynamic stresses in a hollow cylinder or a disc with a hole due to axially symmetric pressure variations. *Trans. Jpn. Soc. Mech. Eng.*, **32**, 709–717.
8 Georgiadis, H. G., Rigatos, A. P., Charalambakis, N. C. (1995) Dynamic stress concentration around a hole in a viscoelastic plate. *Acta Mech.*, **111**, 1–12.
9 Tanimura, S. (1997) Dynamic problems of materials and structures review of the studies. *Trans. Jpn. Soc. Mech. Eng.*, **63**, 2466–2471.
10 Takeda, N. (1997) Impact damage and fracture of advanced composite materials/structures. *Trans. Jpn. Soc. Mech. Eng.*, **63**, 2472–2477.
11 Inoue, H., Kishimoto, K., Aoki, S. (1997) Inverse analysis in impact problems. *Trans. Jpn. Soc. Mech. Eng.*, **63**, 2478–2484.
12 MSC. Software. MARC Volume E: Demonstration Problems. MARC Analysis Research Co., U.S.A., 1997.
13 Murakami, Y., Noda, N.-A., Nisitani, H. (1981) The analysis of stress concentration of a cylindrical bar with a semi-elliptical circumferential notch under tension. *Trans. Jpn. Soc. Mech. Eng.*, **47**, 1194–1205
14 Noda, N.-A., Sera, M., Takase, Y. (1995) Stress concentration factors for round and flat test specimens with notches. *Int. J. Fatigue*, **17**, 163–178.

15 Noda, N.-A., Takase, Y. (1999) Stress concentration formulae useful for any shape of notch in a round test specimen under tension and under bending. *Fatigue Fract. Eng. Mater. Struct.*, **22**, 1071–1082.

16 Noda, N.-A., Takase, Y. (2002) Stress concentration factor formulas useful for all notch shapes in a flat test specimen under tension and bending. *J. Test. Eval.*, **30**, 369–381.

17 Noda, N.-A., Takase, Y. 2010 Fatigue Notch Strength Useful For Machine Design (in Japanese). Nikkan Kogyo Shimbun Ltd., Tokyo.

18 Naitoh, M., Daimaruya, M. (1984) On the dynamic yield of metallic materials under impact loading. *Trans. Jpn. Soc. Mech. Eng.*, **33**, 801–807. (in Japanese)

19 Van Gurp, Marniz; Palmen, Jo (1998) Time-temperature superposition for polymeric blends. *Rheol. Bull.* **67**: 5–8.

20 Ando, M., Noda, N.-A. *et al*. (2014). Impact properties of polydimethylsiloxane copolymerized polycarbonate and application of the time-temperature superposition principle. *Trans. Jpn. Soc. Mech. Eng.* **80**: 814–0149. (in Japanese)